Stress Control of Deep Rift Intrusion at Mauna Loa Volcano, Hawaii

Falk Amelung, *et al.*

Science **316**, 1026 (2007);
DOI: 10.1126/science.1140035

Science (print ISSN 0036-8075; online ISSN 1095-9203) is published weekly, except the last week in December, by the American Association for the Advancement of Science, 1200 New York Avenue NW, Washington, DC 20005.

34. Depth-integrated bacterioplankton biomass and production were not significantly different from the long-term mean at the BATS site. However, as compared to C1, volumetric bacterioplankton biomass and production in A4 were significantly enhanced within the deep chlorophyll a maximum, where diatoms dominated.
35. J. C. Goldman, D. J. McGillicuddy Jr., *Limnol. Oceanogr.* **48**, 1176 (2003).
36. Spectroradiometric observations of photosynthetically available radiation (PAR) in eddy A4 indicated that the depth of 1% of the surface value (a proxy for euphotic zone depth) had a mean of 96 m (SD = 9 m, n = 37 observations), which is nearly identical to that reported at the BATS site (*48*). Findings in C1 were similar, with a mean 1% PAR depth of 97 m (SD = 12 m, n = 49 observations).
37. S. Levitus, *NOAA Professional Paper No. 13* (U.S. Government Printing Office, Washington, DC, 1982).
38. Altimetric data point toward the northern source region for the 1-year period during which the eddy could be tracked (Fig. 1B). However, initial analysis of radioisotope measurements offers conflicting evidence: Radiocarbon data suggest a northern source, whereas tritium data suggest a southern source.
39. Nitrate-to-silicate ratios were similar in cyclone C1 and mode-water eddy A4. Concentrations in the upper euphotic zone were consistent with nitrogen limitation, because excess silicate (~1 to 2 μmol kg^{-1}) was present in waters in which nitrate was depleted (<0.1 μmol kg^{-1}). All of the eddies we studied exhibited a similar tendency for the phosphocline to reside deeper than the nitracline, leading to supra-Redfield nitrate:phosphate ratios just below the euphotic zone. This enigmatic aspect is characteristic of the region (*49*, *50*). Nevertheless, we could find no systematic differences in nitrate-to-phosphate ratios between cyclones and mode-water eddies.
40. A. P. Martin, K. J. Richards, *Deep-Sea Res. II* **48**, 757 (2001).
41. The Martin and Richards model (*40*) predicts the vertical velocity at the base of the layer through which wind stress can be transmitted directly through waves and turbulence (the Ekman layer). Quasigeostrophic theory and models demonstrate that this vertical motion penetrates well into the inviscid interior, diminishing with depth (*51*). We ran a primitive equation model simulation of eddy A4, which indicated that the vertical velocity at the depth of the high-chlorophyll layer was ~90% of the Ekman upwelling velocity. The physical manifestation of this effect is a tendency for upward displacement of the seasonal pycnocline at the eddy center, enhancing the mode-water eddy structure (Fig. 1A).
42. This model also predicts upwelling in the interior of regular anticyclones. An analogous phenomenon has been hypothesized to upwell depressed density surfaces in the interiors of warm-core Gulf Stream rings (*51*), a process that would tend to enhance biological activity associated with their frictional decay (*52*).
43. D. M. Karl, E. A. Laws, P. Morris, P. J. l. B. Williams, S. Emerson, *Nature* **426**, 32 (2003).
44. A. Oschlies, *Global Biogeochem. Cycles* **16**, 1106 (2002).
45. D. J. McGillicuddy, L. A. Anderson, S. C. Doney, M. E. Maltrud, *Global Biogeochem. Cycles* **17**, 1035 (2003).
46. R. C. Dugdale, J. J. Goering, *Limnol. Oceanogr.* **12**, 196 (1967).
47. J. B. Palter, M. S. Lozier, R. T. Barber, *Nature* **437**, 687 (2005).
48. D. A. Siegel *et al.*, *Deep-Sea Res. II* **48**, 1865 (2001).
49. A. F. Michaels *et al.*, *Deep-Sea Res.* **41**, 1013 (1994).
50. J. Wu, W. Sunda, E. A. Boyle, D. M. Karl, *Science* **289**, 759 (2000).
51. W. K. Dewar, G. R. Flierl, *J. Phys. Oceanogr.* **17**, 1653 (1987).
52. P. J. S. Franks, J. S. Wroblewski, G. R. Flierl, *J. Geophys. Res.* **91**, 7603 (1986).
53. R. M. Letelier *et al.*, *Limnol. Oceanogr.* **38**, 1420 (1993).

54. We thank the officers and crews of the R/V *Oceanus* and R/V *Weatherbird II* for their outstanding support during our seagoing operations. R. Leben provided near–real-time altimetric data that were crucial for our adaptive sampling effort. Nutrient samples were processed by the Nutrient Analytical Facility (P. Henderson) at the Woods Hole Oceanographic Institution. Numerical simulations were performed at the National Center for Atmospheric Research's Scientific Computing Division. We thank O. Kosnyreva for expert data analysis and visualization and S. Stasiowski for administrative support. We gratefully acknowledge the efforts of all participants in the EDDIES project, which included a number of BATS technicians. For more information, see http://science.whoi.edu/users/olga/eddies/EDDIES_Project.html. The EDDIES project was funded by NSF's Chemical, Biological, and Physical Oceanography Programs. Additional support for remote sensing aspects (including altimetry and QuikSCAT wind analyses) and high-performance liquid chromatography pigment assays (C. Trees, Center for Hydro-Optics and Remote Sensing) was provided by NASA.

Supporting Online Material

www.sciencemag.org/cgi/content/full/316/5827/1021/DC1
Materials and Methods
Fig. S1
Tables S1 to S3
References

12 October 2006; accepted 13 February 2007
10.1126/science.1136256

Stress Control of Deep Rift Intrusion at Mauna Loa Volcano, Hawaii

Falk Amelung,[1]* Sang-Ho Yun,[2] Thomas R. Walter,[1]† Paul Segall,[2] Sang-Wan Kim[1]

Mauna Loa volcano, Hawaii, deforms by a combination of shallow dike intrusions in the rift zones and earthquakes along the base of the volcano, but it is not known how the spreading is accommodated in the lower part of the volcanic edifice. We present evidence from interferometric synthetic aperture radar data for secular inflation of a dike-like magma body at intermediate depth in the southwest rift zone during 2002 to 2005. Magma accumulation occurred in a section of the rift zone that was unclamped by previous dikes and earthquakes, suggesting that stress transfer plays an important role in controlling subsurface magma accumulation.

Modern volcano-monitoring techniques can detect precursory seismic unrest months to days before an eruption, but information about possible eruption locations is generally not available. Such information is important for hazard assessment and for timely warning of the population for large and populated basaltic shield volcanoes such as Mauna Loa volcano in Hawaii. Forecasting the eruption location requires a better understanding of subsurface magma migration. Here we show that the 2002 to 2005 magma intrusion at Mauna Loa volcano inferred from space-geodetic data is consistent with changes in the stress due to the previous tectonic and magmatic events. This suggests that the stress field within the volcanic edifice is a dominant effect in controlling magma accumulation. Space-geodetic measurements can be used to infer changes to the stress field in the interior and contribute to better forecasts of the response of a volcano to the arrival of new magma from below.

Mauna Loa volcano is the largest and one of the most active volcanoes on Earth. It has produced more than 4 km^3 of lava during the past 150 years (*1*). Most historic eruptions involved the propagation of an eruptive fissure from the summit downrift into the northeast rift zone (NERZ) or into the southwest rift zone (SWRZ) (Fig. 1A). About 30 to 40% of the volcano's subaereal surface has been covered by new lava during the past 1000 years. Thus, a large portion of the island is threatened by lava flows, and it is very important to better estimate where possible eruptions could occur. The last major eruptions occurred in 1950 from the SWRZ and in 1984 from the NERZ. At Mauna Loa, repeated dike intrusions into the rift zone result in seaward motion of the volcano flanks, most of which is believed to be accommodated in form of seismic or aseismic displacement along a decollement fault on the paleo-seafloor at the base of the volcanic edifice at 12- to 14-km depth below the summit. The 1868 magnitude (M) 8 Pahala (*2*) and the 1951 M6.9 Kona earthquakes (*3*) likely ruptured the decollement.

Inflation at Mauna Loa volcano started in May 2002 at the same time when Kilauea volcano increased its rate of lava production (*4*). Subcrustal seismicity increased in 2004 (Fig. 1A). We used interferometric synthetic aperture radar (InSAR) acquired by the Canadian Radarsat-1 satellite between 2001 and early 2006 to obtain a detailed image of the ground deformation associated with the volcanic inflation. InSAR measures the change in distance between the ground and the satellite in radar line-of-sight (LOS) direction. We used imagery with different incidence angles of the radar beam and an average of five to nine interferograms each spanning 3 to 4 years for each viewing geometry (table S1) to obtain averaged LOS velocities for the period May 2002 to end 2005 (*5*). Averaging interferograms increases the signal-to-noise

[1]Rosenstiel School of Marine and Atmospheric Sciences, University of Miami, 4600 Rickenbacker Causeway, Miami, FL 33149, USA. [2]Department of Geophysics, Stanford University, Stanford, CA 94305, USA.

*To whom correspondence should be addressed. E-mail: famelung@rsmas.miami.edu

†Present address: GeoForschungsZentrum Potsdam Section 2.1, Telegrafenberg, 14473 Potsdam, Germany.

ratio of the measurements, which are affected by path delays in the troposphere and by uncertainties in the satellite orbits. InSAR in Hawaii is challenging because repeating weather patterns and up to 4200 m of topography can cause phase contributions of several cycles. Combining multiple viewing geometries better constrains the deformation sources and allows one to estimate the vertical and east component of the velocity field (*6*).

The interferograms show a distinct pattern of ground deformation in the summit area and on the upper flanks of Mauna Loa. For an east-looking interferogram (Fig. 1A), a roughly circular area with a diameter of 10 km west of the rift zone moves toward the radar with a velocity of more than 1 cm/year and maximum velocity of 5 cm/year (yellow-red colors). A smaller area on the southeast flank is moving away from the radar (blue colors). The vertical velocity field is characterized by two lobes of uplift of up to 6 cm/year on either side of the SWRZ, and the east velocity field is roughly symmetric across the SWRZ (Fig. 1B). The symmetry of the ground-velocity field clearly indicates that the principal source of deformation is located within the rift zone.

To understand what causes the observed deformation, we assume elastic material behavior and use geophysical inverse-modeling methods. We first test simple, kinematic models consisting of point (Mogi) sources of inflation and uniform opening dislocations. We find that the data are well explained using a model with a Mogi source southeast of the caldera and an opening dislocation bisecting the caldera and upper SWRZ (*7*). We then consider a more realistic, mechanical model with the magma chamber and dike hydraulically connected and sharing the same excess magma pressure (*8*). The magma chamber is represented as a finite, spherical cavity (*9*) and the dike as a gridlike combination of 1 km by 1 km opening dislocation elements covering 30 km of the rift zone from the surface to the decollement at 14-km depth, subject to a uniform excess-pressure boundary condition. The effect of topography is included in the model (*10*). We invert simultaneously for the opening status of the individual dislocation elements on the dike plane (open or closed) (*11*), for the excess magma pressure, for the location and radius of the spherical cavity, and for phase ramps for each averaged interferogram to account for orbital uncertainties using a Monte Carlo–type simulated annealing algorithm (*12*). The actual opening distribution of the dike-like magma body depends on the configuration of connected dislocation elements.

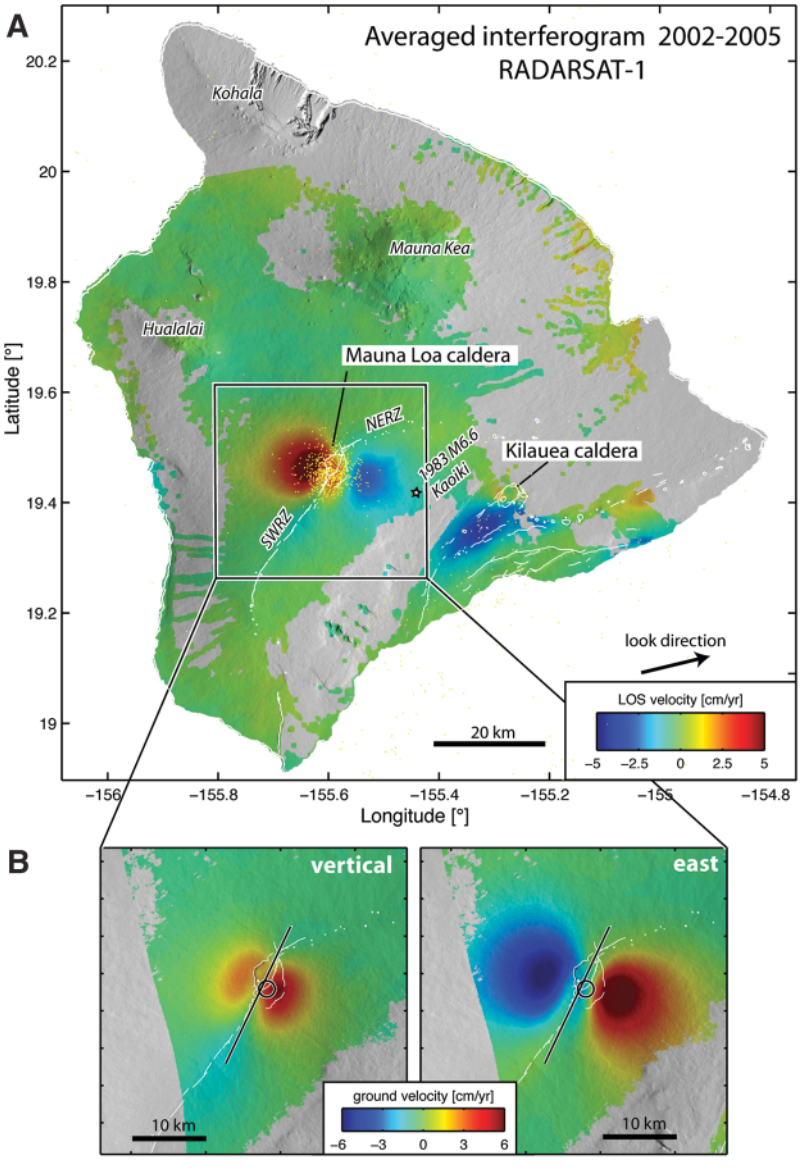

Fig. 1. (A) Averaged 2002 to 2005 satellite radar interferogram of the Big Island of Hawaii showing ground velocity in the radar line-of-sight (LOS) direction. The radar looks toward the east (ascending orbit) with an incidence angle of ~45° on the ground (Standard Beam A6). The star denotes the 1983 Kaoiki earthquake. The seismicity with depth > 20 km and with M > 2.2 is also shown. **(B)** Vertical and east component of the ground-velocity field obtained by combining averaged interferograms from four different viewing geometries. The black line and circle indicate the dike and magma chamber, respectively, of the model in Fig. 2A.

We find that the model magma chamber is under the southeastern caldera margin at 4.7-km depth below the summit (at 0.5-km below sea level) (Fig. 2A); this was also the inferred location of the active reservoir during the 1984 eruption (*13*). The radius of the magma chamber is 1.1 km and the rate of magma excess pressure increase is 1.8 MPa/year. Most of the dike inflation occurs at 4- to 8-km depth along an 8-km-long zone, resulting in an opening of 0.2 to 0.35 m/year (*14*). This model explains about 96% of the data variance. Comparison of the data with the model predictions shows that the data fit is generally very good except near the summit (Fig. 2B). The differences arise because of simplified model assumptions such as a spherical magma chamber and uniform elastic parameters (*15*) and because we did not account for the subtle, pre-2002 subsidence of the summit area detected with the Global Positioning System (*16*) and for the subsidence of the recent intracaldera lava flows due to cooling. We do not include possible fault slip under the flanks because the geometry of the fault plane and the amount of slip are not well constrained (*17*). Other model simplifications are that the dike opening is constrained to take place within the volcanic edifice (to a depth of 14 km below the summit) and that horizontal and vertical variations in the magma pressure go along with variations in the tectonic stress field so that the magma excess pressure is constant.

Although details of the opening distribution of the dike should be interpreted with caution, we conclude that about 80% of the magmatic intrusion occurs in the intermediate and deep section of the rift zone at depth larger than the shallow magma reservoir. This suggests that the volcano operates in a manner similar to that inferred for its neighbor Kilauea with secular magma intrusion into the deep section of the rift zone and occasional dike injection into the shallow section (*18*). Indeed, the intrusion of magma into the deep section of the rift

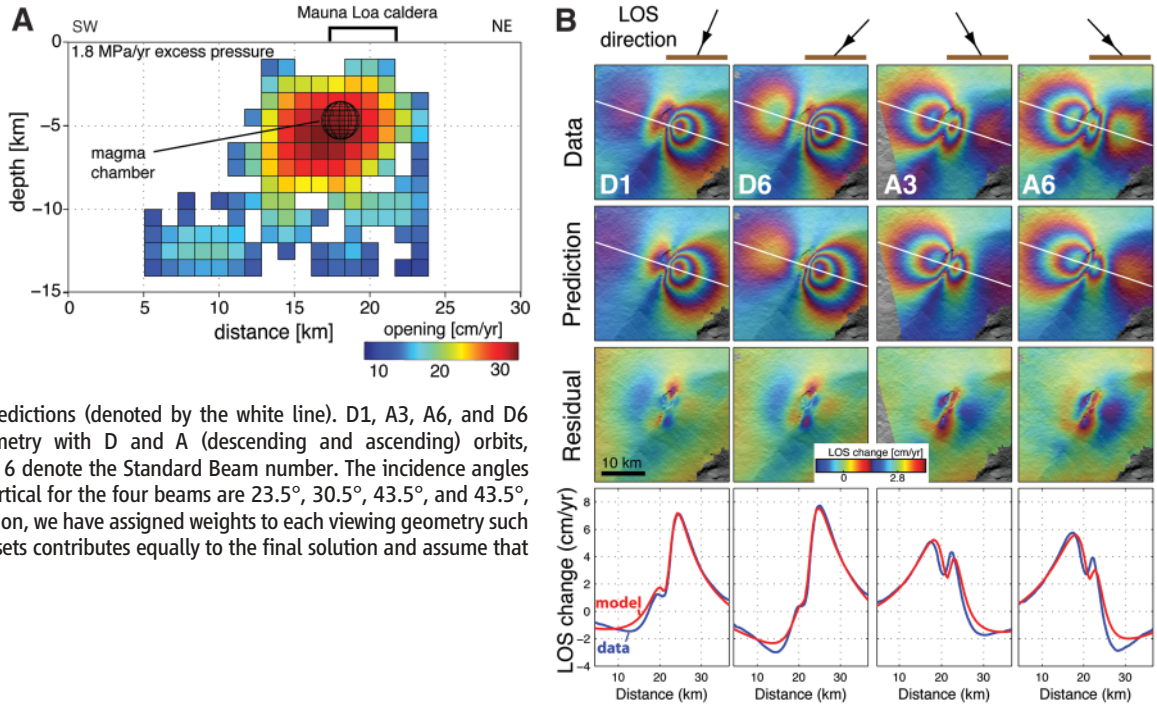

Fig. 2. (**A**) Opening of Mauna Loa's riftzone inferred by inversion of the interferometric data based on a uniform excess–magma pressure model. For the horizontal location of the cross section and magma chamber, see Fig. 1B. (**B**) LOS direction, data, model predictions, residual between data and model prediction, and rift–perpendicular profile of data and model predictions (denoted by the white line). D1, A3, A6, and D6 denote the viewing geometry with D and A (descending and ascending) orbits, respectively, and 1, 3, and 6 denote the Standard Beam number. The incidence angles on the ground from the vertical for the four beams are 23.5°, 30.5°, 43.5°, and 43.5°, respectively. For the inversion, we have assigned weights to each viewing geometry such that each of the four data sets contributes equally to the final solution and assume that the data are uncorrelated.

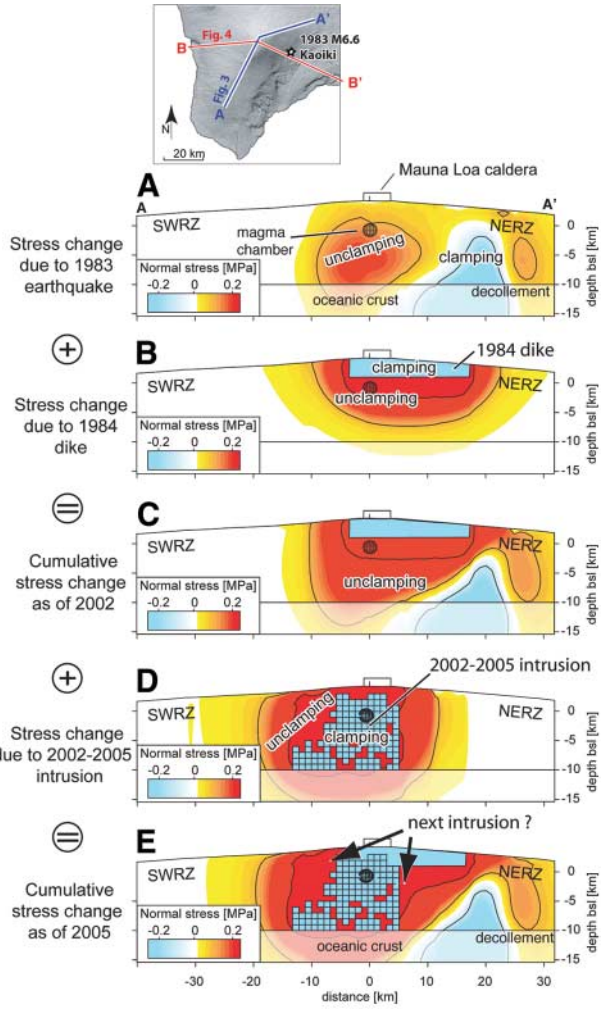

Fig. 3. Changes in normal stress along Mauna Loa's rift zone due to (**A**) the 1983 *M*6.6 Kaoiki earthquake, (**B**) the dike associated with the 1984 eruption, and (**D**) the 2002 to 2005 rift intrusion. (**C** and **E**) The sum of the stress changes from (A) and (B) and (A), (B), and (D), respectively. The color scale is saturated at ±0.2 MPa. Solid lines denote ±0.1 and ±1 MPa contours. The 2002 to 2005 dike intrusion occurs in the area of greatest unclamping. The stress change is resolved in the direction normal to the overall strike of the SWRZ and NERZ along AA′ (see inset). We simulate the earthquake by 0.35 m of strike- and dip-slip displacement along the 225-km^2 fault surface (fig. S3). For the 1984 dike, we use a depth extension of 3 km. This is more than modern, space-geodetic estimates of 1 to 2 km for dikes at Kilauea (*29*), in the Galapagos Islands (*30*), and Piton de la Fournaise (*31*) but less than the estimate of (*13*), which we do not consider reliable because it is based on very few tilt and leveling measurements. It ensures that the dike is well above the magma chamber.

zone is required from simple geometric considerations because all known dike intrusions occurred within the shallow section to a depth of less than 5 km (*19*). The inferred rate of magma accumulation of 21 × 10^6 m^3/year is almost three times the long-term growth rate averaged over the past 4000 years (*19*). As magma intrusion is continuing as of March 2007, albeit at a lower rate, there are no indications that Mauna Loa's magma production rate is waning, as suggested by the decreased eruption rate over the past 50 years (*20*).

We discuss whether the spatial pattern of magma intrusion can be explained by stress transfer and how the 2002 to 2005 intrusion changed the stress field in the interior of the volcano. We first consider changes in the ambient normal stress along the rift zone. We would expect magma intrusion in sections of the rift zone for which the normal stress change resulted in unclamping (positive normal stress change) but no intrusion in clamped sections of the rift zone (negative stress change) (*21*, *22*).

The largest events during the past 25 years were a *M*6.6 earthquake in 1983 and the eruption from the NERZ in 1984. The earthquake occurred in the Kaoiki seismic zone 15 km southeast of the summit (Fig. 1A) and involved right-lateral strike-slip and seaward decollement faulting (*23*). The eruption was associated with a dike propagating from the summit a few kilometers into the SWRZ zone and then into the NERZ from where most of the lava erupted (*1*).

The 1983 earthquake unclamped the upper SWRZ, the upper NERZ, and a section of the NERZ further down the rift (Fig. 3A) (see supporting online material). The 1984 dike unclamped large parts of the rift zone but clamped the section in which it intruded (Fig. 3B). The dike likely relieved stress due to prior events, which is not

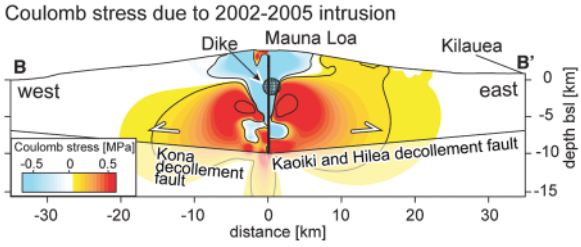

Fig. 4. Changes in Coulomb failure stress resolved for seaward motion parallel to BB′ (see Fig. 3 inset) along 5° inward-dipping faults in a cross section perpendicular to the rift zone. The color scale saturates at ±0.5 MPa. Contours are as in Fig. 3.

included in this stress-change budget. Together, the earthquake and the dike unclamped most of the rift zone (Fig. 3C), with the largest unclamping (by more than 0.2 MPa) occurring in the southern summit section at a depth of 2 to 6 km (the area of inferred magma intrusion during 2002 to 2005).

The 2002 to 2005 intrusion unclamped the rift zone, except in the area of magma intrusion (Fig. 3D). The magnitude of stress change is similar to that for the 1984 dike (Fig. 3B). The inferred opening rate corresponds in places to an opening of 1 m during the 3.3 years covered by our data, even larger in thickness than the 1984 dike. The stress change since 1983 is given by the sum of the stress changes due to the 1983 earthquake, the 1984 dike, and the 2002 to 2005 intrusion (Fig. 3E). The unclamping is most pronounced in the shallow section of the upper SWRZ and in the intermediate-depth section of the NERZ.

The stress-change modeling shows that the magma intrusion during 2002 to 2005 occurred into the most-unclamped section of the rift zone since 1983 (*24*). This observation is notable because it suggests that the stress changes due to the 1983 and 1984 events influenced, if not controlled, the accumulation of the magma. Consequently, if we can constrain the deformation sources to reliably estimate changes in the stress field, we can forecast the location for the accumulation of new magma and possibly of eruptions based on the stress-change models. Obviously, other factors also contribute, such as local stress heterogeneities associated with the magma conduits and magmatic factors such as the size and compressibility of the reservoir feeding the intrusion and the vesicularity and density of the magma, but our results suggest that stress changes due to prior events are the dominant effect.

The historic eruptions of Mauna Loa were fissure eruptions associated with dikes injected into the shallow rift zone. After the 2002 to 2005 intrusion, the most favorable stress conditions for the propagation of shallow dikes occurred in the upper SWRZ (Fig. 3E). Thus, according to the stress-change models, this is the most likely location for a new dike injection and possibly for an eruption. The last eruption from this section of the rift zone occurred in 1950. A new eruption from the SWRZ would be consistent with the previously observed pattern of alternating eruptions between the NERZ and the SWRZ (*25*, *26*).

We also estimate how the 2002 to 2005 intrusion has influenced the flank stability and affected the potential for slumping of the flanks and for decollement earthquakes under the flanks of the volcano. We evaluate changes of the Coulomb failure stress (*27*, *28*) resolved for seaward motion along nearly horizontal faults in a cross section roughly perpendicular to the rift zone. An increase of the Coulomb failure stress encourages faulting, and a decrease discourages faulting, respectively. In the central section of the volcanic edifice, the changes in Coulomb failure stress are negative above sea level but positive below sea level (Fig. 4). The strongest stress changes occur at about 5- to 7-km depth under the southeast flank because of the combined effect of rift intrusion and chamber inflation. In the shallow southeast flank, the stress changes are also positive. The 2002 to 2005 intrusion stabilized the summit section of the volcanic edifice, discouraging landslide-type motion, but strongly destabilized the deep part of the edifice, making it prone to earthquakes along horizontal faults such as the decollement. Changes in Coulomb failure stress are 0.1 MPa and larger in most places of the seismogenic decollement fault. Bearing in mind that stress changes as low as 0.01 MPa can trigger earthquakes (*28*), the below–sea level portion of Mauna Loa has clearly been destabilized by the magma intrusion. Faulting along the decollement fault would be consistent with the previously observed pattern of alternating rift intrusions and decollement earthquakes (*22*). Indeed, aseismic motion along subhorizontal faults may already have been occurring during 2002 to 2005, but it is difficult to constrain with surface measurements.

Our analysis leads to a new model for Mauna Loa's magmatic system. During 2002 to 2005, most of the magma generated in the mantle, possibly at the depth of the subcrustal seismicity, rose into the deep and intermediate section of the rift zone, whereas only a small percentage rose into the shallow magma chamber. Intrusion of the magma changes the stress field within the volcanic edifice and encourages dike propagation into the shallow SWRZ and faulting along subhorizontal faults in most parts of the volcanic edifice, including along the decollement fault. Mauna Loa volcano likely exhibits a cyclic behavior such that deformation due to earthquakes and intrusions encourages new intrusions elsewhere in the rift zone and fault slip under the flanks.

References and notes

1. J. P. Lockwood *et al.*, in *U.S. Geol. Surv. Prof. Pap. 1350*, R. W. Decker, T. L. Wright, P. H. Stauffer, Eds. (1987), vol. 1, pp. 537–570.
2. M. Wyss, *Bull. Seismol. Soc. Am.* **78**, 1450 (1988).
3. F. W. Klein, T. L. Wright, *U.S. Geol. Surv. Prof. Pap. 1623* (2000).
4. A. Miklius, P. Cervelli, *Nature* **421**, 229 (2003).
5. Averaged LOS velocities are obtained by dividing the sum of the interferograms by the cumulative time of the interferograms since 12 May 2002. The averaged rates cover slightly different time periods since the beginning of the inflation (3.41, 3.30, 3.37, and 3.26 years for Standard Beams A3, A6, D1, and D6, respectively), but we verified that this does not affect our conclusions. We neglect the subtle deflation of the summit area before May 2002 (*16*), which according to 1997 to 2002 InSAR data, occurred at a rate below the measurement noise.
6. T. J. Wright, B. E. Parsons, Z. Lu, *Geophys. Res. Lett.* **31**, L01607 (2004).
7. In this model, the depth of the Mogi source is 3.2 km; the dislocation is nearly vertical, 10 km long at 3- to 11-km depth with an opening rate of 25 cm/year. The volume-change rates are $\Delta V_{mogi} = 2.7 \times 10^6$ m^3/year and $\Delta V_{dike} = 20.6 \times 10^6$ m^3/year.
8. Materials and methods are available as supporting material on *Science* Online.
9. D. F. McTigue, *J. Geophys. Res.* **92**, 12931 (1987).
10. C. A. Williams, G. Wadge, *J. Geophys. Res.* **105**, 8103 (2000).
11. S. Yun, P. Segall, H. Zebker, *J. Volcanol. Geotherm. Res.* **150**, 232 (2006).
12. P. Cervelli, M. H. Murray, P. Segall, Y. Aoki, T. Kato, *J. Geophys. Res.* **106**, 11217 (2001).
13. D. J. Johnson, in *Geophys. Monograph 92*, J. M. Rhodes, J. P. Lockwood, Eds. (American Geophysical Union, Washington, DC, 1995), pp. 127–143.
14. The volume-change rates are $\Delta V_{McTigue} = 0.2 \times 10^6$ m^3/year and $\Delta V_{dike} = 21.6 \times 10^6$ m^3/year. For the model coordinates, see fig. S1. The pseudo-95% confidence intervals for the depth, radius, and excess-pressure rate range from 3.5 to 7 km, 0.8 to 1.3 km, and 1.2 to 3.1 MPa/year, respectively (fig. S2). Only 1% of the magma accumulation occurs in the shallow reservoir, but its location and volume-change rate are relatively well constrained because the data resolve shallow sources well. The difference in the inferred volume-change rate for the magma chamber compared with that of the previous model occurs because of different treatment of the dike-like magma body.
15. If the volcano has shallow, mechanically soft layers, then the magmatic sources are deeper and stronger than inferred here with a homogeneous model.
16. A. Miklius *et al.*, in *U.S. Geol. Surv. Open-File Rep. 1425* (2005).
17. Deep-rift opening and near-rift decollement slip result in a similar surface deformation pattern, making it difficult to distinguish between the two types of deformation sources on the basis of surface measurements.
18. S. Owen *et al.*, *J. Geophys. Res.* **105**, 18983 (2000).
19. P. W. Lipman, in *Geophys. Monograph 92*, J. M. Rhodes, J. P. Lockwood, Eds. (American Geophysical Union, Washington, DC, 1995), pp. 45–80.
20. There were only two major eruptions with a volume larger than 100×10^6 m^3 since 1950 compared with 15 major eruptions between 1841 and 1949 (*20*, *22*).
21. This is consistent with recent results suggesting that external decompression of a magma chamber (an instantaneous pressure drop) leads to a delayed pressure increase (*22*).
22. T. R. Walter, F. Amelung, *J. Geophys. Res.* **111**, B05204 (2006).
23. M. D. Jackson, E. T. Endo, P. T. Delaney, T. Arnadottir, A. M. Rubin, *J. Geophys. Res.* **97**, 8775 (1992).
24. Events before 1983 also influenced the stress state along the rift zone, but we do not have enough information to reliably estimate their effects. The 1950 eruption was associated with a dike extending from the caldera into the SWRZ that could explain the lack of appreciable shallow intrusion into the upper SWRZ from 2002 to 2005. The dike feeding the 1975 eruption was likely only a few kilometers long (*1*), and the resulting stress changes were much smaller than for the 1984 dike. Stress changes due to events at Kilauea volcano are small because static stress changes fall off with distance r as $1/r^3$. An earthquake at twice the distance causes one-eighth as many stress changes.
25. T. A. Jaggar, *Nature* **101**, 54 (1918).
26. J. P. Lockwood, P. W. Lipman, in *U.S. Geol. Surv. Prof. Pap. 1350*, R. W. Decker, T. L. Wright, P. H. Stauffer, Eds. (1987), vol. 1, pp. 509–535.

27. The change in Coulomb failure stress is defined as $\Delta CFS = \Delta\sigma_s + \mu\Delta\sigma_n$, where $\Delta\sigma_s$ is the change in shear stress, $\Delta\sigma_n$ is the change in effective normal stress, and μ is the coefficient of effective internal friction (*28*). We use $\mu = 0.4$.
28. G. C. P. King, R. S. Stein, J. Lin, *Bull. Seismol. Soc. Am.* **84**, 935 (1994).
29. S. Owen *et al.*, *Geophys. Res. Lett.* **27**, 2757 (2000).
30. S. Jonsson *et al.*, *Geophys. Res. Lett.* **26**, 1077 (1999).
31. Y. Fukushima, V. Cayol, P. Durand, *J. Geophys. Res.* **110**, B03206 (2005).
32. We thank NASA's Earth Science program and the NSF's Geophysics program for funding, the Alaska satellite facility for conducting the data acquisition, and the Hawaii Volcano Observatory for their support. This work is based on Radarsat imagery, a satellite operated by the Canadian Space Agency. Two reviewers provided constructive comments. Center for Southeastern Tropical Advanced Remote Sensing (CSTARS) contribution #11.

Supporting Online Material
www.sciencemag.org/cgi/content/full/316/5827/1026/DC1
Material and Methods
Table S1
Figs. S1 to S4
References

17 January 2007; accepted 3 April 2007
10.1126/science.1140035

FT Protein Movement Contributes to Long-Distance Signaling in Floral Induction of *Arabidopsis*

Laurent Corbesier,[1] Coral Vincent,[1]* Seonghoe Jang,[1]* Fabio Fornara,[1] Qingzhi Fan,[2] Iain Searle,[1] Antonis Giakountis,[1] Sara Farrona,[1] Lionel Gissot,[1] Colin Turnbull,[2] George Coupland[1]†

In plants, seasonal changes in day length are perceived in leaves, which initiate long-distance signaling that induces flowering at the shoot apex. The identity of the long-distance signal has yet to be determined. In *Arabidopsis*, activation of *FLOWERING LOCUS T* (*FT*) transcription in leaf vascular tissue (phloem) induces flowering. We found that *FT* messenger RNA is required only transiently in the leaf. In addition, FT fusion proteins expressed specifically in phloem cells move to the apex and move long distances between grafted plants. Finally, we provide evidence that FT does not activate an intermediate messenger in leaves. We conclude that FT protein acts as a long-distance signal that induces *Arabidopsis* flowering.

Perception of day length takes place in the leaf, whereas flowers are formed by the shoot apical meristem at the apex of the shoot (*1*, *2*). A long-distance signal, called florigen or the floral stimulus, has been demonstrated to be transmitted through the phloem vascular system from the leaves to the meristem, although the identity of this signal has remained unclear since the 1930s. Molecular-genetic approaches in *Arabidopsis* have defined a regulatory pathway that promotes flowering in response to long days (LDs) and have suggested how this pathway responds to day length (*3*–*5*). Under LDs, the CONSTANS (CO) transcriptional regulator activates transcription of *FLOWERING LOCUS T* (*FT*) in the vascular tissue of leaves (*6*–*8*). *FT* encodes a small protein with similarity to RAF-kinase inhibitors that acts at the meristem together with the transcription factor FD to activate transcription of the floral meristem identity gene *APETALA1* (*7*, *9*–*11*). *FT* is expressed in the leaves in response to photoperiod, but FT protein

[1]Max Planck Institute for Plant Breeding Research, Carl von Linne Weg 10, D-50829 Cologne, Germany. [2]Division of Biology, Imperial College London, Wye Campus, Wye, Kent TN25 5AH, UK.

*These authors contributed equally to this work.
†To whom correspondence should be addressed. E-mail: coupland@mpiz-koeln.mpg.de

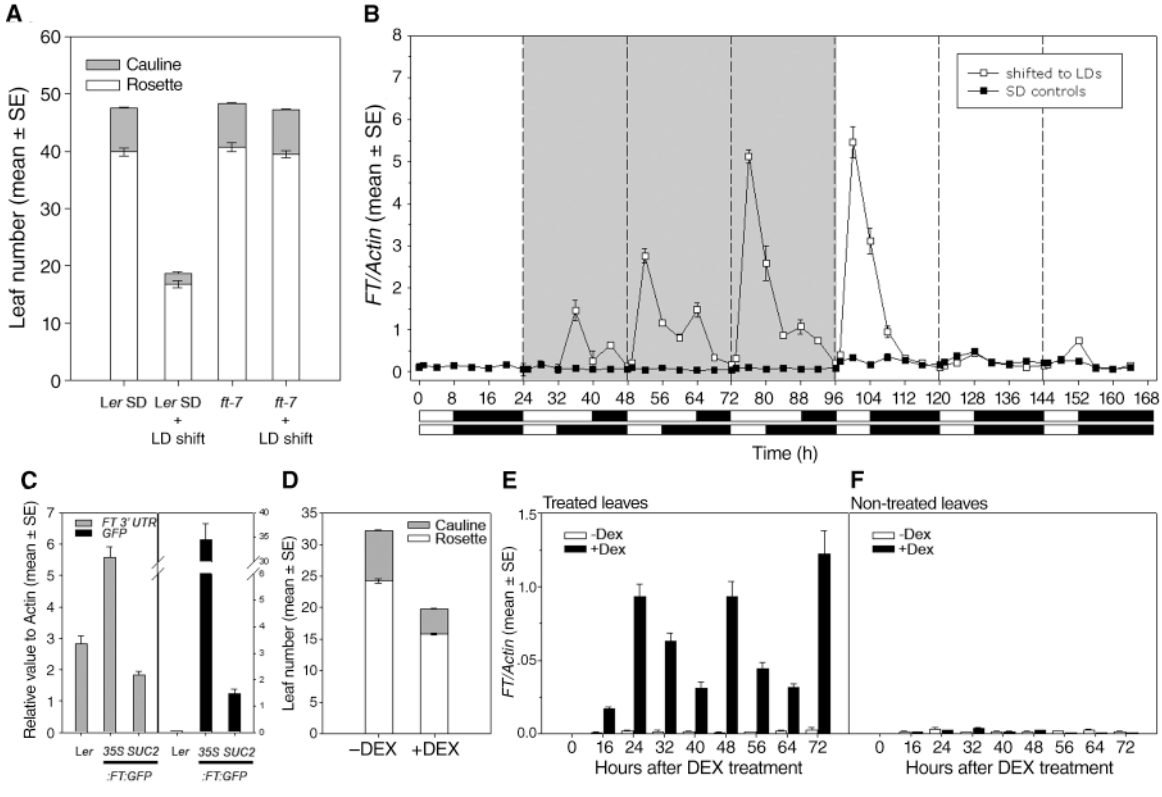

Fig. 1. Regulation of *FT* mRNA in leaves during flowering. (**A**) Flowering time of wild-type *Ler* and *ft-7* plants grown for 2 weeks under SD and exposed to three inductive LDs before return to SDs. (**B**) Expression of *FT* mRNA during 7 days comprising one SD followed by three LDs and then three subsequent SDs. *FT* mRNA expression in the SD-grown controls is also shown. RNA was tested every 4 hours. The inserted three LDs are shaded. Below the graph, bars show the duration of day (white) and night (black) for the shift experiment (top) and the control experiment (bottom). (**C**) Endogenous *FT* mRNA [FT 3′ untranslated region (UTR)] and *FT:GFP* mRNA (GFP) expression in 14-day-old *Ler*, *35S:FT:GFP*, and *SUC2:FT:GFP* plants. (**D**) Leaf number at flowering of *CO:CO:GR*, *co-2* plants treated (+DEX) or not treated (–DEX) with dexamethasone. Plants were grown for 2 weeks in SD conditions and then shifted to LDs for 4 days. Dexamethasone was applied during the LD treatment. (**E** and **F**) *FT* mRNA expression in treated (E) and nontreated (F) leaves of *CO:CO:GR* plants.